2.4 μm Cutoff AlGaAsSb/InGaAsSb Phototransistors for Shortwave IR Applications

Tamer F. Refaat
Applied Research Center,
Old Dominion University
12050 Jefferson Avenue,
Newport News, VA 23606
Phone (757) 269-5641
Email trefaat@jlab.org

M. Nurul Abedin
Passive Sensor Systems Branch
NASA Langley Research Center
5 Dryden Street, MS 468
Hampton, VA 23681

Oleg V. Sulima
Department of Electrical and Computer Engineering,
University of Delaware,
140 Evans Hall
Newark, DE 19716

Krishna Swaminathan
Department of Electrical and Computer Engineering,
University of Delaware,
140 Evans Hall
Newark, DE 19716

Syed Ismail
Chemistry and Dynamics Branch
NASA Langley Research Center
21 Langley Boulevard, MS 401A
Hampton, VA 23681

Upendra N. Singh
Systems Engineering Directorate
NASA Langley Research Center
5 North Dryden Street, MS 433
Hampton, VA 23681

2.4 μm Cutoff AlGaAsSb/InGaAsSb Phototransistors for Shortwave IR Applications

Abstract

Shortwave infrared detectors are critical for several applications including remote sensing and optical communications. Several detectors are commercially available for this wavelength range, but they lack sufficient gain, which limits their detectivity. The characterization results of an AlGaAsSb/ InGaAsSb phototransistor for shortwave IR application are reported. The phototransistor is grown using molecular beam epitaxy technique. Spectral response measurements showed a uniform responsivity between 1.2 and 2.4 μm region with a mean value of 1000 A/W. A maximum detectivity of 3.4×10^{11} cmHz$^{1/2}$/W was obtained at 2 μm at -20^{o}C and 1.3 V.

1- Introduction

Shortwave IR detectors are important for several applications, including atmospheric remote sensing, optical communications and absorption spectroscopy[1-3]. The availability of laser sources at 1.0, 1.3, 1.5 and 2.0 μm drives the need for high quality quantum detectors operating at the same wavelengths[1, 4]. Although extended wavelength InGaAs and HgCdTe detectors can provide such sensitivity, they lack sufficient responsivity due to the absence of internal gain mechanisms. Besides, system complexity increases toward longer wavelengths due to cooling requirement. This limits the devices signal-to-noise ratio (SNR) and therefore applicability for some instrumentation.

InGaAsSb quaternary material show promising performance for shortwave IR detectors[5-12]. Development of InGaAsSb based p-n and p-i-n junctions detectors were reported with relatively lower noise and higher speed. Shellenbarger et. al. pointed out that a back-illuminated p-n junction had a narrow spectral band centered near 2 μm, which has the advantage of reducing the background signal and increasing the detector dynamic range[11]. Avalanche photodiode (APD) structure increases the SNR over the pn and p-i-n structures. This attributed to the internal avalanche gain, which increases the device responsivity while maintaining both high bandwidth and dynamic range. AlGaAsSb/InGaAsSb APDs with separate absorption and multiplication (SAM) regions structure have been reported at least

by two research groups. Andreev et. al. presented SAM-APDs operating between 1.2 and 2.3 μm wavelength and having multiplication gains of 20 and 100 at room temperature and 78K, respectively, while biased with 27V[6]. Using similar SAM-APD structure Sulima et al reported an improved device, by increasing the responsivity to 43 A/W at 2.1 μm and lowering the avalanche voltage to 6.7V at room temperature[12]. In the same paper the avalanching regime was described in InGaAsSb/GaSb APDs, and a responsivity of 8.9 A/W at a wavelength of 2.0 μm was measured at 7.5 V also at room temperature[12]. Practically, using a quaternary material for photodetector fabrication increases the flexibility to tailor the detection wavelength, but increases the device processing complexity. This might limit the commercial availability of such devices.

Recently high gain heterojunction phototransistors (HPT) have been developed using InGaAsSb/AlGaAsSb material by liquid phase epitaxy (LPE)[13-15]. The advantage of these HPTs is their optimization around the 2 μm wavelength with high internal gain, which leads to high responsivity and high SNR. For example at 2 μm wavelength device responsivity of 2650 A/W, corresponding to 2737 internal gain at -20^{o}C and -4V bias voltage was measured[14]. The detectivity calculation of this LPE-grown HPT indicated 3.9×10^{11} cmHz$^{1/2}$/W, which corresponds to 4.6×10^{-14} W/Hz$^{1/2}$ noise-equivalent-power (NEP). Although these devices indicated excellent performance, they had fundamental limitation of the cutoff wavelength due to the LPE growth process[16]. Compared to LPE, molecular beam epitaxy (MBE) provides better control over doping levels, composition and width of the AlGaAsSb and InGaAsSb layers, especially with regard to abrupt heterojunctions[15, 16]. Therefore, devices with a longer cutoff wavelength, covering larger spectral range, could be fabricated. In this paper, we present the characterization results of a newly developed, MBE-grown InGaAsSb/ AlGaAsSb HPT, operating in the wavelength range between 1.0 and 2.6 μm.

2- Phototransistor Growth and Structure

The HPT, shown schematically in Figure 1, is composed of $Al_{0.25}Ga_{0.75}As_{0.02}Sb_{0.98}$ and $In_{0.18}Ga_{0.82}As_{0.17}Sb_{0.83}$ layers consistent with GaSb lattice matching conditions[18]. At room-temperature the layers bandgaps are 1.0 eV and 0.54 eV, respectively. The layers are grown on an n^{+}-GaSb (001) substrate and include a 0.1 μm-thick n^{+}-GaSb contact layer, 0.5 μm thick n-type AlGaAsSb emitter, 0.8 μm-thick p-type composite base consisting of AlGaAsSb (0.3μm) and InGaAsSb (0.5μm) layers, and a 1.5 μm-thick n-type InGaAsSb collector. HPT with different mesa and active areas were defined using photolithography and wet chemical etching, as listed in Table I. A backside planar and frontside

annular ohmic contacts (together with a bonding pad) were deposited by electron beam evaporation of Au/Ge. A polyimide coating (HD Microsystems PI-2723 photodefinable polyimide resin) was spun on the front surface of the device. The polyimide served several functions including planarisation of the top surface, mesa isolation, and edge passivation. After dicing 1×1 mm^2 pieces with a single device in the middle, the diced pieces were mounted to TO-18 headers using silver conducting epoxy for the bottom contact and wire-bonding the upper pad. No antireflection coatings were applied[16].

3- Characterization Results and Discussion

Several HPT samples were characterized to evaluate the performance of the new device structure gown with the MBE technique. Characterization of the HPT included dark current, spectral response and noise measurements. Based on these measurements, figure-of-merits were calculated including the device quantum efficiency, gain and detectivity, D*.

3.1- Dark Current

Figure 2 shows the dark current density variation with the bias voltage for different samples and also at different temperatures for sample M1-a2. Dark current density was obtained by I-V measurements in dark conditions using a modulator Semiconductor Characterization system. Device mesa area was used to normalize the dark current for current density, as presented in the figure. Two distinctive regions were observed from the dark current variation with temperature. The first region, where the dark current density is lower than 0.5 A/cm^2, is characterized by higher temperature dependence. This attributed to the domination of the diffusion and generation-recombination dark current components, which are strongly dependent on temperature[19]. The second region, with dark current density above 0.5 A/cm^2, tunneling current component is dominant, which has less temperature dependence[19]. Dark current variation with temperature is consistent using different samples with different limit for the two regions. Absence of any intersection between the dark current curves at different temperatures indicates the absence of any avalanche gain. Therefore, any observed gain is mainly due to transistor action.

3.2- Spectral Response and Quantum Efficiency

The spectral response of the HPT was measured using the substitution method in reference to a 3×3 mm2 PbS calibrated detector[15, 20]. Spectral resolution of 20 nm was obtained in the 1.0 to 2.7 μm

wavelength range. Figure 3 shows the spectral response of the HPT sample M1-a2, operating at zero bias voltage and different temperatures. Assuming no gain at this bias level, the figure also compares the measurements to constant quantum efficiency contours. The spectral response cuts on around 1.1 μm, with an almost flat response between 1.2 and 2.2 μm, then cuts off around 2.3 μm. Quantum efficiency as high as 70% was achievable using moderate cooling to -20^{o}C. One advantage of the new device is the uniformity of the quantum efficiency at wavelengths in the 1.2 - 2.0 μm range. Focusing on some wavelengths of interest, such as 1.3, 1.5 and 2.0 μm, Figure 4 shows the quantum efficiency variation with temperature from 100 to -192.6^{o}C.This indicates that the device is fully operational within a large temperature range, with reproducible results. An optimum operating temperature of -45^{o}C maximizes the quantum efficiency, independent on the wavelength. According to the InGaAsSb composition given in the previous section, the cutoff wavelength is about 2.4 μm at room temperature. Cooling down the device shifts the cutoff to shorter value according to the variation of the energy bandgap with temperature, as indicated in Figure 4.

Operating at room temperature, Figure 5 shows the spectral response of different HPT samples at different bias voltages. High responsivity is observed at relatively low bias voltage (about 1.4V), indicating high device gain. For example, at 2 μm and 20^{o}C the responsivity of sample M1-a2 increases from 0.75 A/W to 1105 A/W by increasing the bias voltage from 0 to 1.4 V. This indicates an internal device gain of 1475. Figure 6 shows the gain variation with bias voltage for the same sample at different temperatures. Further increase in the device bias leads to saturation of the gain at a certain level dependent on the operating temperature. Experimentally, the bias voltage is limited to the current carrying capacity of the device as determined by the dark current measurements.

3.3- Device Noise and Figure-of-Merit

The HPT noise was measured using a low-frequency spectrum analyzer (Stanford Research Systems; SR570) in the frequency range from 0 to 100 kHz. For a certain operating conditions, in terms of bias voltage and temperature, and after subtracting the system noise, the total detector noise was averaged in the frequency band. Figure 7 shows the noise variation with bias voltage obtained for different samples at 20^{o}C and at lower temperature of -20^{o}C for sample M1-a2. The HPT noise increases by increasing the device bias voltage. Reducing the device temperature slightly reduces the noise. This might be attributed to the device dark current shot noise, which is the dominating noise

source for these devices. Dark current shot noise is dependent on the device gain, which is higher for the device operating at lower temperature and above 1 V, as presented in Figure 6.

In the processing of the new MBE grown HPT, the ratio of sensitive to mesa area was increased, compared to the previously LPE grown devices[13, 16]. This leads to increase the SNR of the new devices. Figure 8 shows the detectivity (D*) as a function of wavelength compared to the background limited D* and that of an LPE-grown HPT sample[14]. At wavelength shorter than 1.8 μm a higher D* was obtained from the MBE samples, while extending the detection wavelength to 2.4 μm, for the same operating temperature. For a certain device, reducing the temperature increases the D* due to both increase in the gain and decrease in noise. D* as high as 3.4×10^{11} cmHz$^{1/2}$/W was obtained using sample M1-a2 around 2 μm at -20^{o}C and 1.3 V. A maximum room temperature detectivity of 1.6×10^{11} cmHz$^{1/2}$/W was obtained from sample, M1-c8.

4- Conclusion

In this paper the characteristics of newly developed InGaAsSb/AlGaAsSb phototransistors were presented. The new devices were grown using the molecular beam epitaxy (MBE) technique and are sensitive for the 1.0 to 2.6μm wavelength range. The devices exhibit high gain due to the transistor action, which results in high responsivity and enhanced signal-to-noise ratio. Responsivity increases from 0.75 A/W to 1105 A/W by increasing the bias voltage only form 0 to 1.4 V, indicating an internal gain of 1475.1. The new devices are capable of operation in a wide temperature range, between 100 to -192.6^{o}C. Although extreme temperature operation affects the performance, the samples recover these conditions with reproducible results and without damage. D* as high as 3.4×10^{11} cmHz$^{1/2}$/W was obtained around 2 μm wavelength at -20^{o}C. Room temperature D* of 1.6×10^{11} cmHz$^{1/2}$/W at 2 μm was obtained, suggesting simple applicability without complex cooling requirements.

References

1. P. Ambrico, A. Amodeo, P. Girolamo, and N. Spinelli, “Sensitivity analysis of differential absorption lidar measurements in the mid-infrared region,” *Applied Optics*, **39**(36), 6847–6865, 2000.
2. J. Benoit, M. Boulou, G. Soulage, A. Joullie, and H. Mani, “Performance evaluation of GaAlAsSb/GaInAsSb SAM-APDs for high bit rate transmission in the 2.5μm wavelength region”, *Journal of Optical Communication*, **9**(2), 55–58, 1988.

3. B. Carter, E. Shaw, J. Olesberg, W. Chan, T. Hasenberg, and M. Flatte, “High detectivity InGaAsSb pin infrared photodetector for blood glucose sensing”, *Electronics Letters*, **36**(15), 1301–1303, 2000.
4. J. Yu, A. Braud and M. Petros, “600-mJ, double-pulse 2-μm laser”, *Optics Letters*, **28**(7), 540-542, 2003.
5. Srivastava, A.; DeWinter, J.; Caneau, C.; Pollack, M.; and Zyskind, J.: High Performance GaInAsSb/GaSb p-n Photodiodes for the 1.8-2.3 μm Wavelength Range. *Applied Physics Letters*, **48**(14), 903–904, 1986.
6. A. Andreev, M. A. Afrailov, A. N. Baranov, M. A. Mirsagatov, M. P. Mikhailov, and Y. P. Yakovlev, “GaInAsSb/GaAlAsSb avalanche photodiode with separate absorption and multiplication regions,” *Soviet Technical Physics Leters*, **14**, 435–437, 1988.
7. Andreev, I.; Afrailov, M.; Baranov, A.; Konnikov, S.; Mirsagatov, M.; Mikhailova, M.; Salata, O.; Umanskii, V.; Filaretova, G.; and Yakovlev, Y.: Ultrafast GaInAsSb p-i-n Photodiode for the Spectral Interval 1.5-2.3 μm. *Soviet Technical Phys. Letters*, **15**(4), 253–254, 1989.
8. Mikhailova, M. P.; Andreev, I. A.; Baranov, A. N.; Mel’nikov, S. V.; Smortchkova, Y. P.; and Yakovlev, Y. P.: Low-Noise GaInAsSb/GaAlAsSb SAM Avalanche Photodiode in the 1.6-2.5 μm Spectral Range. *Proceedings of SPIE*, **1580**, 308–312, 1991.
9. Zhang, B.; Zhou, T.; Jiang, H.; Ning, Y.; and Jin, Y.: GaInAsSb/GaSb Infrared Photodetectors Prepared by MOCVD. *Electr. Letters*, vol. 31, no. 10, 1995, pp. 830–832.
10. Li, A.; Zhong, J.; Zheng, Y.; Wang, J.; Ru, G.; Bi, W.; and Qi, M.: Molecular Beam Epitaxial Growth, Characterization and Performance of High-Detectivity GaInAsSb/GaSb PIN Detectors Operating at 2.0 to 2.6 μm. *J. of Crystal Growth*, vol. 150, 1995, pp. 1375–1378.
11. Shellenbarger, Z. A.; Mauk, M. G.; Cox, J.; South, J.; Lesko, J.; Sims, P.; and DiNetta, L.: GaInAsSb and InAsSbP Photodetectors for Mid-Infrared Wavelengths. *Proceedings of SPIE*, vol. 3379, 1998, pp. 354–360.
12. O.V. Sulima, M.G. Mauk, Z.A. Shellenbarger, J.A. Cox, P.E. Sims, S. Datta, and S.B. Rafol, “Uncooled low-voltage AlGaAsSb/InGaAsSb/GaSb avalanche photodetectors”, IEE Proceedings-Optoelectronics, 151, 1 (2004).
13. O.V. Sulima, T.F. Refaat, M.G. Mauk, J.A. Cox, J. Li, S.K. Lohokare, M.N. Abedin, U.N. Singh & J. A. Rand, “AlGaAsSb/InGaAsSb phototransistors for spectral range around 2 μm”, Electronics Letters, Vol. 40, No. 12, page 766-767, June 2004.

14. T. Refaat N. Abedin, O. Sulima, S. Ismail and U. Singh, "AlGaAsSb/InGaAsSb phototransistors for 2-μm remote sensing applications", *Optical Engineering,* **43**(7), 1647-1650, 2004.
15. N. Abedin, T. Refaat, O. Sulima and U. Singh, "Recent development of Sb-based phototransistors in the 0.9- to 2.2-μm wavelength range for applications to laser remote sensing", *International Journal of High Speed Electronics and Systems*, **16**(2), 567-582, 2006.
16. O. Sulima, K. Swaminathan, T. Refaat, N. Faleev, A. Semenov, V. Solov' ev, S. Ivanov, N. Abedin, U. Singh and D. Prather, "2.4 μm cutoff wavelength AlGaAsSb/InGaAsSb phototransistors", *Electronic Letters,* **42**(1), 2006.
17. N. Abedin, T. Refaat, O. Sulima, S. Ismail & U. Singh, "Two-micron detector development using Sb-based material systems", Sixth Annual Earth Science Technology Conference, ESTC 2006, NASA's Earth Science Technology Office (ESTO), College Park, Maryland, June 2006.
18. S. Adachi, "Band gaps and refractive indices of AlGaAsSb, GaInAsSb, and InPAsSb: key properties for a variety of the 2-4-μm optoelectronic device applications", *Journal of Applied Physics,* **61**(10), 4869-4876, 1987.
19. S. Forrest, "Performance of InGaAsP photodiodes with dark current limited by diffusion, generation recombination and tunneling", *IEEE Journal of Quantum Electronics*, **17**(2), 217-226, 1981.
20. T. Larason, S. Bruce, and A. Parr, "Spectroradiometric detector measurements: part I ultraviolet detectors and part II visible to near-infrared detectors", *NIST Special Publications*, 250– 41, 1998.

Table I: HPT samples grown by MBE technique and the corresponding mesa and active areas diameters, D_m and D_a, respectively.

Sample	**D_m [μm]**	**D_a [μm]**
M2-d1	100	75
M1-c8	300	200
M1-a2	400	300
M1-e1	1100	1000

Figure Captions

Figure 1: Structure of the heterojunction phototransistor samples grown by molecular beam epitaxy.

Figure 2: Dark current variation with bias voltage for different samples, obtained at 20^{o}C and for sample M1-a2 obtained at different temperatures (100^{o}C top curve to -20^{o}C bottom curve, with 20^{o}C temperature step).

Figure 3: Spectral response of the HPT sample M1-a2, operating at zero bias voltage and different temperatures compared to constant quantum efficiency counters.

Figure 4: Quantum efficiency variation with temperature at three common wavelengths for the HPT sample M1-a2 operating at zero bias voltage. Also the variation of the 50% cut-off wavelength with temperature is shown for the same device.

Figure 5: Spectral response for different HPT samples with different area, obtained at 20^{o}C at various bias voltages.

Figure 6: Gain variation with bias voltage at four different temperatures of 100, 60, 20 and -20^{o}C for HPT sample M1-a2.

Figure 7: Noise variation with bias voltage for different HPT samples with different area, obtained around room temperature. Also the same characteristic is presented for sample M1-a2 at -20^{o}C.

Figure 8: Detectivity calculation for different HPT samples at different operating conditions, compared to previously presented LPE device (200 and 400 μm sensitive area and mesa diameters, respectively, operating at -20^{o}C and 4.0 V, see reference 14) and background limited D* at 20^{o}C.

Figure 1

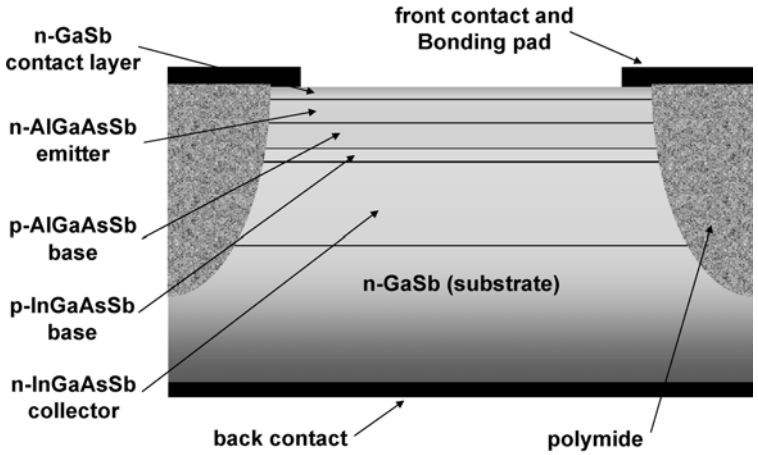
front contact and
Bonding pad
n-GaSb
contact layer
n-AlGaAsSb
emitter
p-AlGaAsSb
base
p-InGaAsSb
base
n-InGaAsSb
collector
n-GaSb (substrate)
back contact
polymide

Figure 2

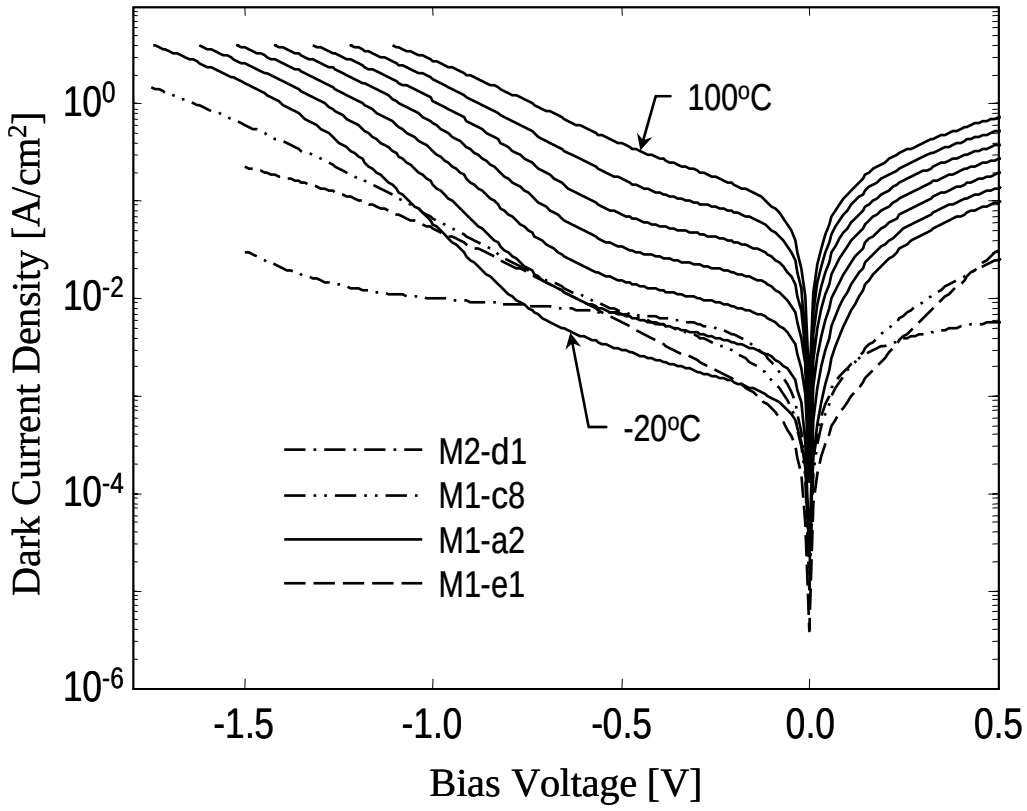
Dark Current Density [A/cm^2]
10^0
10^{-2}
10^{-4}
10^{-6}
100°C
-20°C
M2-d1
M1-c8
M1-a2
M1-e1
-1.5
-1.0
-0.5
0.0
0.5
Bias Voltage [V]

Figure 3

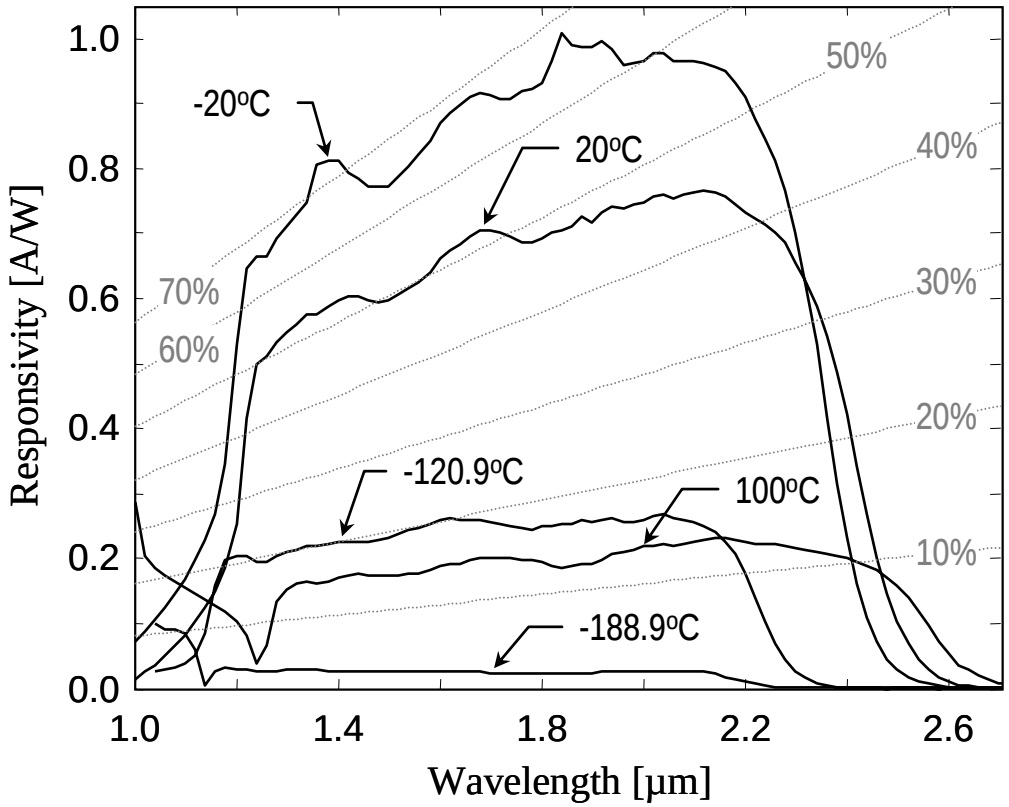
Responsivity [A/W]
Wavelength [μm]
1.0
0.8
0.6
0.4
0.2
0.0
1.0
1.4
1.8
2.2
2.6
-20°C
20°C
-120.9°C
100°C
-188.9°C
70%
60%
50%
40%
30%
20%
10%

Figure 4

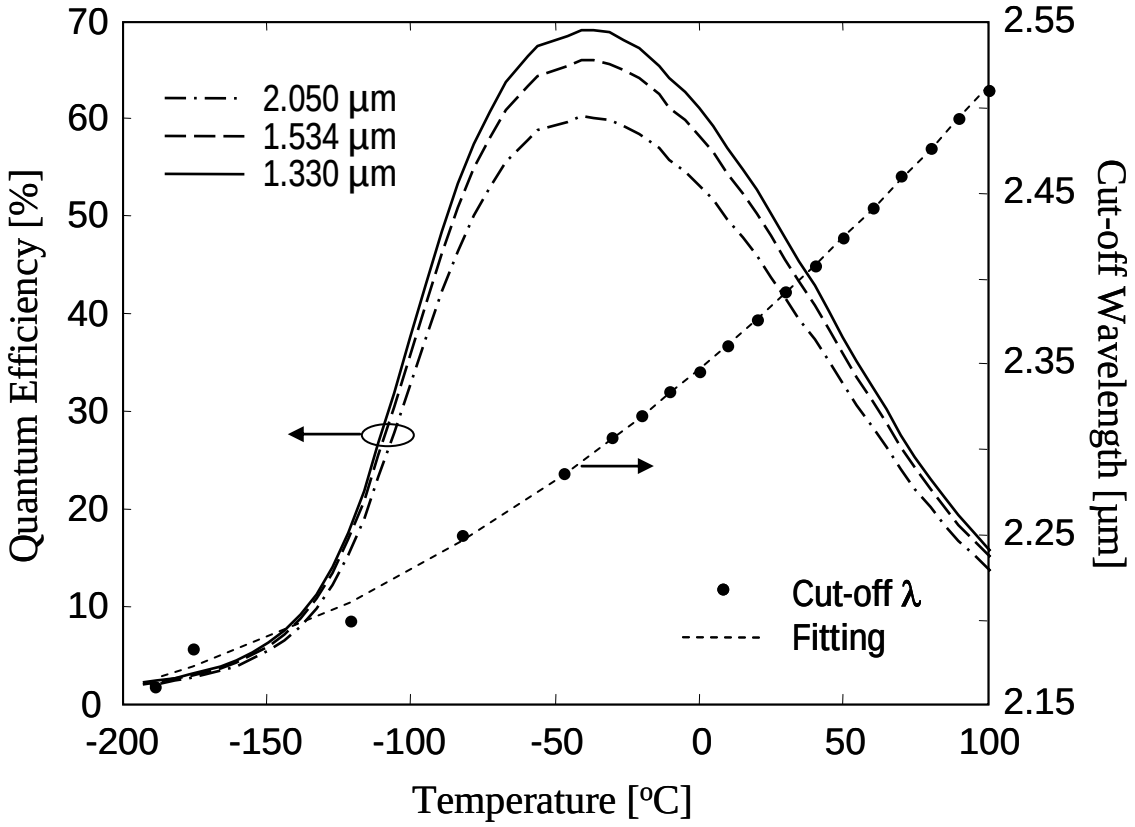
Quantum Efficiency [%]
Cut-off Wavelength [μm]
Temperature [°C]
2.050 μm
1.534 μm
1.330 μm
Cut-off λ
Fitting
70
60
50
40
30
20
10
0
2.55
2.45
2.35
2.25
2.15
-200
-150
-100
-50
0
50
100

Figure 5

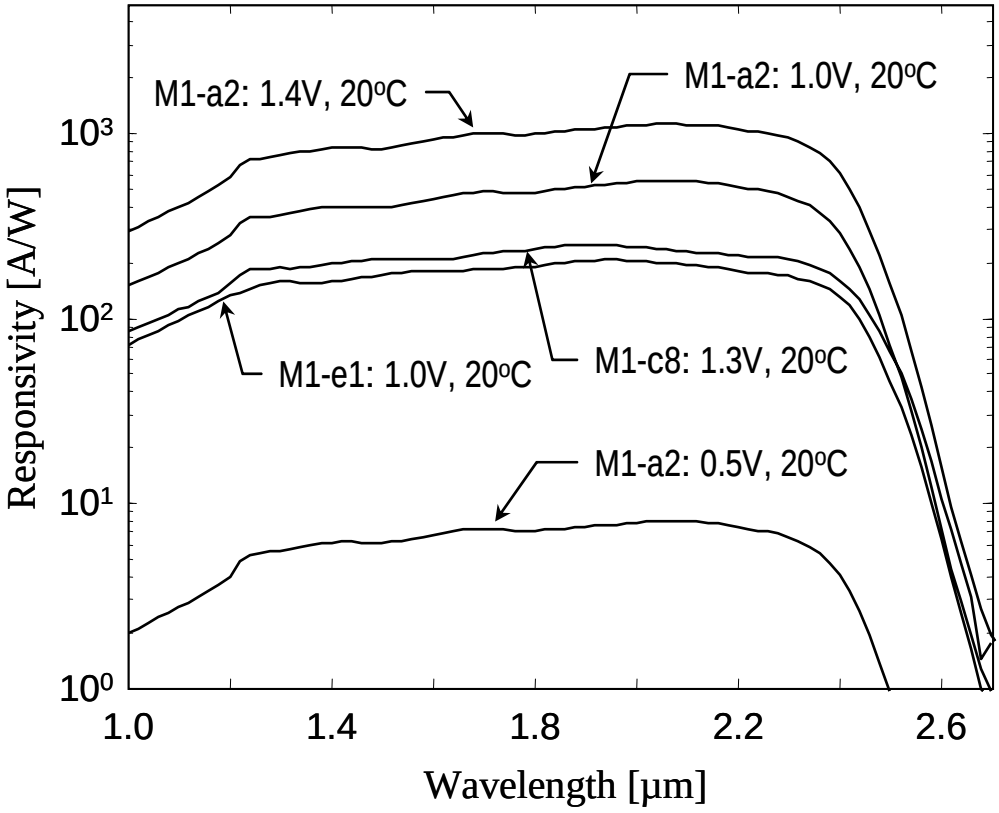
M1-a2: 1.4V, 20°C
M1-a2: 1.0V, 20°C
M1-e1: 1.0V, 20°C
M1-c8: 1.3V, 20°C
M1-a2: 0.5V, 20°C
Responsivity [A/W]
10³
10²
10¹
10⁰
1.0
1.4
1.8
2.2
2.6
Wavelength [μm]

Figure 6

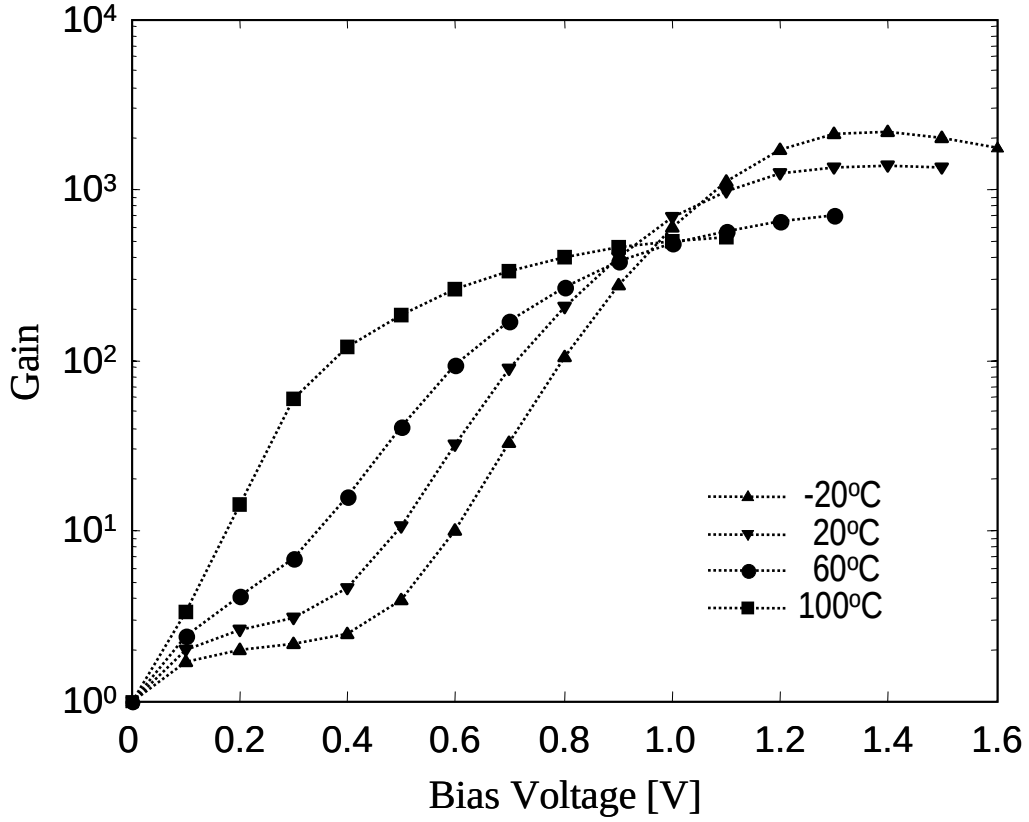

Figure 7

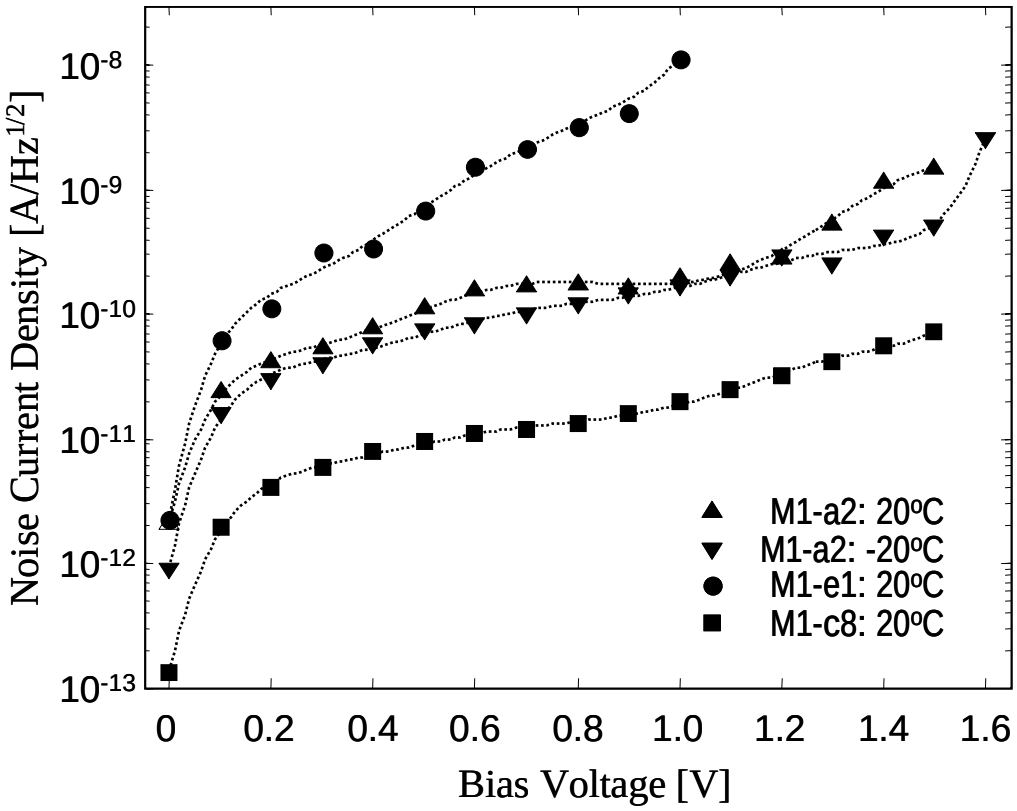
Noise Current Density [A/Hz^1/2]
10^-8
10^-9
10^-10
10^-11
10^-12
10^-13
0
0.2
0.4
0.6
0.8
1.0
1.2
1.4
1.6
Bias Voltage [V]
M1-a2: 20°C
M1-a2: -20°C
M1-e1: 20°C
M1-c8: 20°C

Figure 8

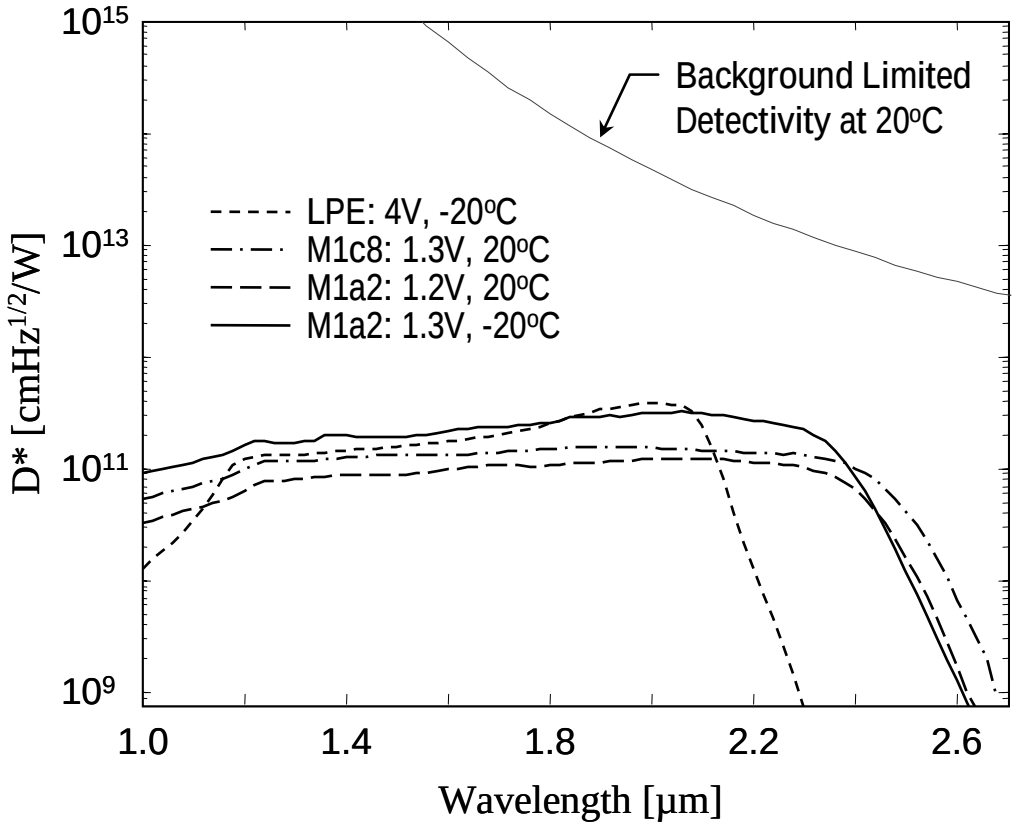
Background Limited
Detectivity at 20°C
LPE: 4V, -20°C
M1c8: 1.3V, 20°C
M1a2: 1.2V, 20°C
M1a2: 1.3V, -20°C
D* [cmHz^1/2/W]
10^15
10^13
10^11
10^9
1.0
1.4
1.8
2.2
2.6
Wavelength [μm]